Oncogene
https://doi.org/10.1038/s41388-020-1238-z

ARTICLE

The proprotein convertase furin is a pro-oncogenic driver in *KRAS* and *BRAF* driven colorectal cancer

Zongsheng He[1] · Lieven Thorrez[2] · Geraldine Siegfried[3] · Sandra Meulemans[1] · Serge Evrard[3,4] · Sabine Tejpar[5] · Abdel-Majid Khatib[3] · John W. M. Creemers[1]

Received: 23 December 2019 / Revised: 19 February 2020 / Accepted: 19 February 2020
© The Author(s), under exclusive licence to Springer Nature Limited 2020

Abstract

Mutations in *KRAS* and/or *BRAF* that activate the ERK kinase are frequently found in colorectal cancer (CRC) and drive resistance to targeted therapies. Therefore, the identification of therapeutic targets that affect multiple signaling pathways simultaneously is crucial for improving the treatment of patients with *KRAS* or *BRAF* mutations. The proprotein convertase furin activates several oncogenic protein precursors involved in the ERK-MAPK pathway by endoproteolytic cleavage. Here we show that genetic inactivation of furin suppresses tumorigenic growth, proliferation, and migration in *KRAS* or *BRAF* mutant CRC cell lines but not in wild-type *KRAS* and *BRAF* cells. In a mouse xenograft model, these *KRAS* or *BRAF* mutant cells lacking furin displayed reduced growth and angiogenesis, and increased apoptosis. Mechanistically, furin inactivation prevents the processing of various protein pecursors including proIGF1R, proIR, proc-MET, proTGF-β1 and NOTCH1 leading to potent and durable ERK-MAPK pathway suppression in *KRAS* or *BRAF* mutant cells. Furthermore, we identified genes involved in activating the ERK-MAPK pathway, such as *PTGS2*, which are downregulated in the *KRAS* or *BRAF* mutant cells after furin inactivation but upregulated in wild-type *KRAS* and *BRAF* cells. Analysis of human colorectal tumor samples reveals a positive correlation between enhanced furin expression and *KRAS* or *BRAF* expression. These results indicate that furin plays an important role in *KRAS* or *BRAF*-associated ERK-MAPK pathway activation and tumorigenesis, providing a potential target for personalized treatment.

UNCORRECTED PROOF

Introduction

Colorectal cancer (CRC) is the second leading cause of cancer deaths amongst men and women [1]. Although complete surgical removal of tumors may be curative in the early stages of CRC, systemic therapy is still the most common way to treat advanced CRC by targeting signaling pathways related to the progression of CRC. Several investigations have uncovered a series of signaling pathways involved in the initiation and progression of CRC [2, 3]. These include the MAPK, PI3K, WNT, TGF-β, P53, and DNA mismatch-repair signaling pathways. Modulation of these signaling pathways has provided a wide range of pharmacological targets. For instance, cetuximab interferes with both MAPK and PI3K signaling pathways and reduces the risk of progression of metastatic CRC [4]. Like many other drugs, however, single targeting of these signaling pathways always have limited effects, as CRC often harbors mutations in multiple signaling pathways. This highlights the urgent need for new therapeutic targets that can interfere in multiple signaling pathways related to tumor progression. Q1 –Q4

These authors contributed equally: Abdel-Majid Khatib, John W. M. Creemers

Supplementary information The online version of this article (https://doi.org/10.1038/s41388-020-1238-z) contains supplementary material, which is available to authorized users.

✉ John W. M. Creemers
john.creemers@kuleuven.be

[1] Laboratory of Biochemical Neuroendocrinology, Department of Human Genetics, KU Leuven, Leuven, Belgium

[2] Interdisciplinary Research Facility, Department of Development and Regeneration, KU Leuven, Campus Kulak Kortrijk, Kortrijk, Belgium

[3] INSERM, LAMC, UMR, Allée Geoffroy St Hilaire, 1029 Pessac, France

[4] Institut Bergonié, Bordeaux, France

[5] Digestive Oncology Unit, Department of Oncology, University Hospitals Leuven, Leuven, Belgium

Another obstacle limiting the efficacy of CRC treatments is the disease's heterogeneity, with temporal and spatial differences in genetic mutations, epigenetic regulation, and tumor microenvironment, which lead to different responses and different patient survival outcomes with the same treatments. More than half of CRCs harbor either *KRAS* or *BRAF* mutations and are often refractory to approved targeted therapies [5]. Emerging evidence suggests that the failure of these targeted drugs can be attributed to primary and acquired drug resistance [5]. The different mutational status of *KRAS* and *BRAF*, as important effectors in the MAPK signaling pathway, accounts at least partly for the primary resistance to targeted treatments in patients with CRC. Compensatory loops within the MAPK pathway and cross-regulation with other pathways like PI3K pathway are major reasons for acquired drug resistance. Therefore, new therapeutic targets will have to be studied to take this heterogeneity or targeting of multiple signaling pathways into account.

Furin together with six other members (PC1/3, PC2, PC4, PACE4, PC5/6 and PC7) constitute the proprotein convertase (PC) family that cleaves proproteins carboxyterminal of basic motifs such as Arg-X-Lys/Arg-Arg [6]. Within this family, PC1/3, PC2, and PC4 exhibit a tissue-specific distribution, whereas furin, PACE4, PC5/6, and PC7 are expressed in a broad range of cell lines and tissues. The latter PCs have partially overlapping substrates and functions because of their concurrent expression in cell lines and tissues [7]. However, it is still largely unknown which substrate is cleaved by which PC and to what extent there is redundancy in cleavage. Furin is the first discovered and so far the best-characterized PC. In vitro and in vivo studies have shown that it is involved in the cleavage of many substrates including growth factors and its receptors, adhesion molecules, angiogenic factors, and extracellular matrix proteins [7, 8]. Since several of these furin substrates are involved in activating multiple tumor-associated signaling pathways including WNT, NOTCH, MAPK, PI3K, and TGF-β pathways, furin can be expected to play a crucial role in tumorigenesis [9]. In addition, overexpression has been observed in various cancer types including squamous cell carcinomas [10], head and neck carcinoma [11], ovarian cancer [12], and rhabdomyosarcoma [13]. Furthermore, several reports have demonstrated that the ablation of furin inhibited tumor-related capabilities, such as sustained proliferation, angiogenesis, immune evasion, and metastatic dissemination [9, 13–15]. This indicates that furin could be an ideal target for cancer treatments including CRC. It has already been shown that the inactivation of furin leads to the downregulation of the PI3K-AKT pathway by interfering with proteolytic cleavage of the proIGF1R in a CRC cell line [16], but it is still unclear whether other furin substrates and their related pathways are involved in inhibition of CRC. Furthermore, the therapeutic potential of furin inactivation in the context of *KRAS* or *BRAF* mutation status is currently unknown.

In this study, we used clustered regularly interspaced short palindromic repeats (CRISPR)/Cas9 to knock out furin in CRC cells with *KRAS* (DLD1) or *BRAF* (HT29) mutations, or wild type (WT) for *KRAS* and *BRAF* (HCA7) to study the tumorigenic role of furin in concert with mutated *KRAS* or *BRAF*. We have analyzed the processing of potential furin substrates and the effect on MAPK and other oncogenic signaling pathways. Furthermore, we have analyzed oncogenic parameters of these cells, both in vitro and in vivo. Finally, RNA-seq experiments were performed to obtain insight into the genetic heterogeneity of the different CRC lines.

Results

Altered furin expression in human colon cancer with *KRAS* or *BRAF* mutations

At all steps of tumor development and progression, potential furin substrates play an important role (Fig. 1a). Therefore, we analyzed the expression of human furin in colon cancer tissue by immunostaining. As illustrated in Fig. 1b, furin was expressed specifically in the colon crypts of non-cancerous colon tissues. In all the analyzed cancerous tissues with *KRAS* or *BRAF* mutations, furin showed a greatly spread expression throughout the tumor that coincided with loss of crypts and alteration of the epithelial structure of the colon tissue. This indicates that the presence of furin in *KRAS* or *BRAF* mutant tumors may play a role in their malignant phenotype. Accordingly, using TCGA (The Cancer Genome Atlas) data of human CRC with the *KRAS* or *BRAF* expression [17], we identified a positive correlation between the expression of furin and *KRAS* ($r = 0.38$, Spearman's rank correlation coefficient, $p = 2.3e{-}14$) or *BRAF* ($r = 0.28$, $p = 4.3e{-}8$) (Fig. 1c).

Furin repression inhibits the proteolytic maturation of colorectal carcinogenesis-related furin substrates

To investigate the therapeutic potential of furin inactivation on the malignant phenotype of *KRAS* or *BRAF* mutant tumors, we genetically modified the furin gene in colon cancer cells with *KRAS* (DLD1) or *BRAF* (HT29) mutation as well as in colon cancer cells with WT *KRAS* and *BRAF* (HCA7) using CRISPR/Cas9. We selected a sgRNA targeting exon 2 of furin that encodes the translation initiation site, the signal peptide, and part of the prodomain of furin (Fig. 2a). Deletion of this exon leads to the functional inactivation of furin [18]. Three independent KO clones

UNCORRECTED PROOF

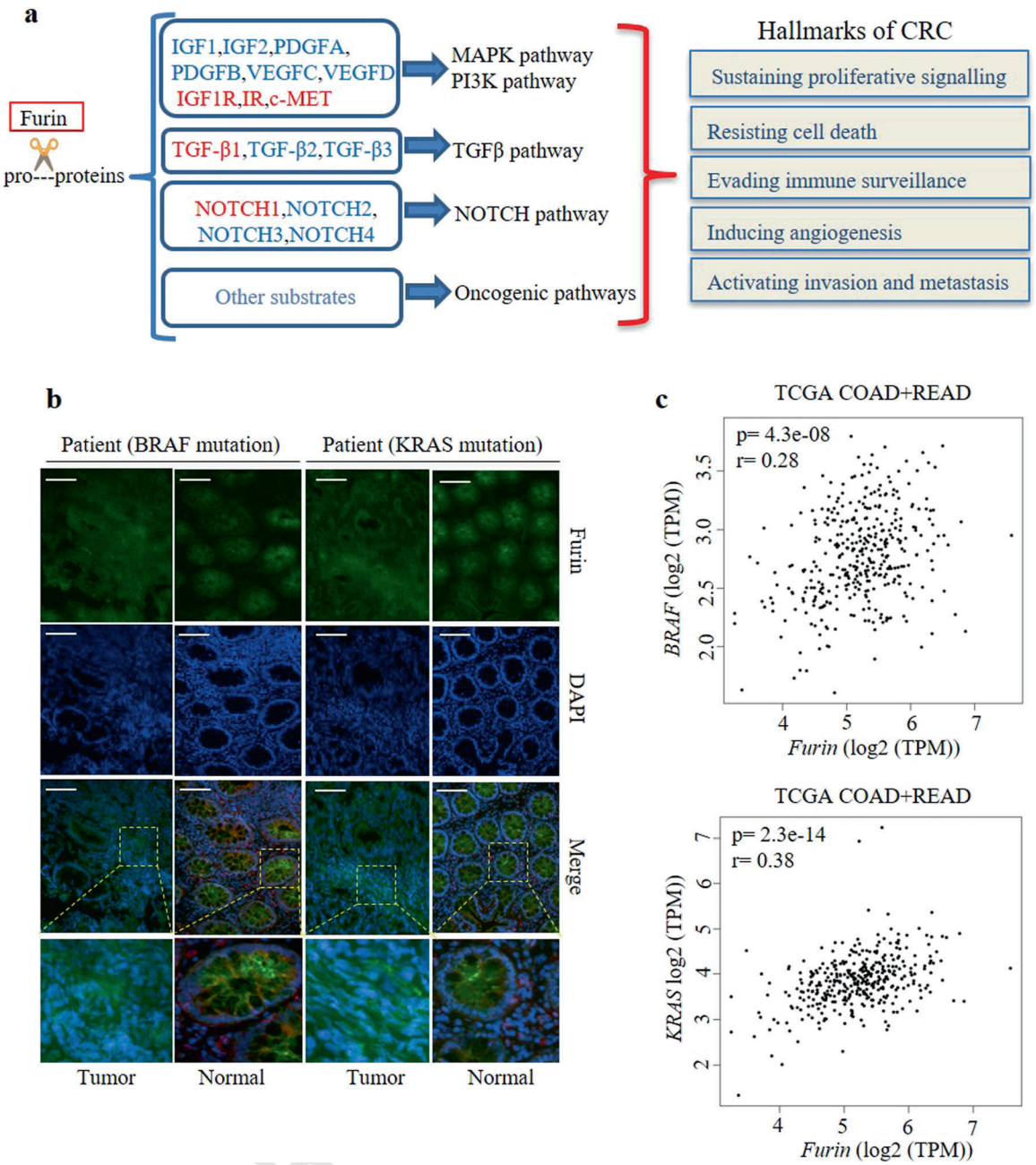

Fig. 1 Altered expression pattern of furin in *KRAS* or *BRAF* mutant CRC tumor samples. a Schematic showing the important role of potential furin substrates in different stages of carcinogenesis. IGF1/IGF2 insulin-like growth factor 1/2, PDGFA/B platelet-derived growth factor A/B, VEGFC/D vascular endothelial growth factor C/D, IGF1R insulin-like growth factor 1 receptor, IR insulin receptor, c-MET hepatocyte growth factor receptor, TGF-β1/2/3 transforming growth factor beta-1/2/3, NOTCH1/2/3/4 neurogenic locus notch homolog protein 1/2/3/4. Potential furin substrates in red were investigated in this study. **b** The expression pattern of furin in cancerous colon tissue and paired normal colon tissue. Representative immunofluorescent image of furin from tumor tissue of CRC patients (scale bar: 100 μm). The regions in the yellow squares were further enlarged in the bottom panels. **c** Correlation of *furin* expression with *BRAF* or *KRAS* expression in primary colorectal tumors. Expression data are from the TCGA collection of human colorectal adenocarcinomas. Each dot represents one sample. The strength of the correlation was determined using the Spearman's correlation coefficient (*r*), and the two-tailed *P* value was calculated. COAD colon adenocarcinoma, READ rectum adenocarcinoma, TPM transcripts per million.

were generated for each colon cancer cell line (DLD1/KO1-3, HCA7/KO1-3, and HT29/KO1-3 cells) and inactivation of furin was verified by sequencing and western blotting (Fig. 2b). No compensatory upregulation of any of the other ubiquitously expressed PC5/6, PACE4, and PC7 was found (Fig. S1a).

We subsequently examined the processing of several potential furin substrates involved in colon cancer,

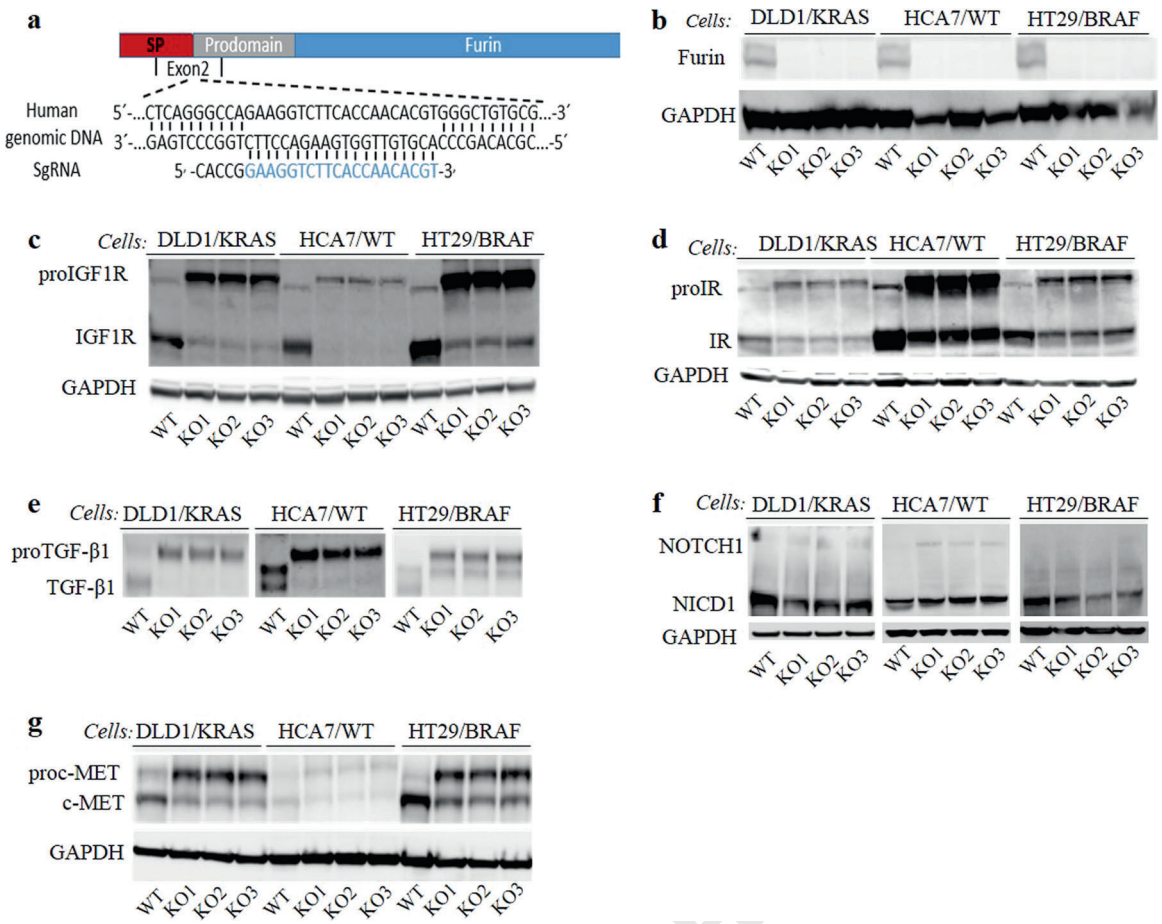

Fig. 2 Inactivation of furin inhibits processing of multiple oncoproteins in CRC cell lines. a Schematic representations of the targeting locus of exon 2 in the human furin gene and the single guide RNA (SgRNA) sequence (Blue) used for CRISPR/Cas9 genome editing. SP signal peptide. **b** Immunoblotting of cell extracts from WT and three independent furin KO clones for each cell line. Immunoblot analysis of selected furin substrates including proIGF1R (**c**), proIR (**d**), proTGF-β1 (**e**), NOTCH1 (**f**), and proc-MET (**g**) in furin KO CRC cells. Both pro- and mature form of the proteins are indicated. GAPDH served as a loading control, except for TGF-β1, which was analyzed in the medium. All results were representative of three experiments.

UNCORRECTED PROOF

including IGF-I receptor (IGF1R), insulin receptor (IR), TGF-β1, and NOTCH1. Immunoblotting analysis show that the IGF-IR precursor is processed into the mature form in all WT cells, but maturation was blocked in all KO cells (Fig. 2c). Similarly, the proIR was almost completely processed into IR in all WT cells, while proIR accumulated in KO cells (Fig. 2d). Notably, IR shows much higher protein levels in HCA7/WT than DLD1/*KRAS* and HT29/*BRAF* cells. We next assessed proteolytic maturation of TGF-β1 in these colon cancer cells. Mature TGF-β1 could not be detected in any of the KO cells, while proTGF-β1 accumulated (Fig. 2e), confirming that furin is the major convertase of proTGF-β1 in all these cells. We observed an upregulation of TGF-β1 mRNA in HCA7/WT KO cells but not in DLD1/*KRAS* and HT29/*BRAF* KO cells (Fig. S1b).

Furin is also involved in the cleavage of the NOTCH1 signaling pathway by participating in releasing NOTCH1 intracellular domain (NICD) [19]. Immunoblotting results showed that the absence of furin leads to a slight increase in uncleaved NOTCH1, but the impact on the amount of NICD was limited. In DLD1/*KRAS* KO and HT29/*BRAF* KO cells, the amount of NICD was slightly decreased, while in HCA7/WT KO cells it was slightly increased (Fig. 2f). c-MET is a proto-oncogene that encodes the hepatocyte growth factor receptor protein. After binding with its ligand, HGF, this RTK activates a wide range of different cellular signaling pathways that mediate proliferation, motility, migration and invasion. c-MET is involved in the initiation of colon cancer and implicated in the acquired resistance to targeted therapies especially with liver metastasis [20, 21]. We observed that high levels of c-MET were detected in DLD1/*KRAS* and HT29/*BRAF* cells, while reduced levels were found in HCA7/WT cells (Fig. 2g). As for the previous candidate substrates, a clear reduction of the processed form was observed in the KO cells with a concomitant increase in proc-MET.

Taken together, these results demonstrate that furin plays a crucial, non-redundant role in the processing of proIGF1R,

proIR, proTGF-β1, and proc-MET. In addition, it is involved in the processing of NOTCH1, but other PCs provide redundancy to a variable degree. Finally, we observed no notable differences in the degree of processing of substrates between the three different CRC lines lacking furin, although the expression of the substrates varied considerably.

Furin inactivation reduces ERK/MAPK signaling pathways and regulates the expression of downstream effectors in KRAS or BRAF mutant CRC cells

As a key effector of *KRAS* or *BRAF* oncogenic properties, the ERK/MAPK signaling pathway is one of the main drivers in colorectal carcinogenesis with *KRAS* or *BRAF* mutation [22]. We observed a strong reduction in ERK phosphorylation in mutated *KRAS* (DLD1/KO1-3) and *BRAF* (HT29/KO1-3) cells following inactivation of furin (Fig. 3a and Fig. S2a). In contrast, the cells with WT *KRAS* and *BRAF* showed a highly activated ERK/MAPK pathway, which was even slightly increased in furin KO cells (HCA7/KO1-3). We observed a modest decrease in the activation of the PI3K/AKT pathway in the KO cells of DLD1/*KRAS* and HT29/*BRAF* cells, albeit only statistically significant in DLD1/*KRAS* KO cells (Fig. 3a and Fig. S2b). In contrast, we detected no autophosphorylation of AKT at either Thr308 or Ser473 sites in HCA7/WT cells. All in all, inactivation of furin inhibits the activity of the ERK/MAPK and PI3K/AKT pathways in mutated *KRAS* or *BRAF* cells but not in WT *KRAS* and *BRAF* cells.

To evaluate the effect of impaired processing of furin substrates on ERK/MAPK activation directly, we first assessed IGF1R and IR activation using IGF1 and insulin, respectively (Fig. 3b–d and Fig. S2c–e). As anticipated, addition of exogenous IGF1 or insulin activated the IGF1R and IR, respectively, and enhanced the activity of ERK/MAPK and PI3K/AKT pathways in all control cells. In contrast, furin KO cells showed significantly reduced phosphorylated IGF1R and IR as well as activated pERK and pAKT compared with control cells.

To investigate the effect of furin inactivation on the TGF-β1 signaling pathway, we analyzed the phosphorylation level of SMAD2 (Fig. 3e). Immunoblotting analysis revealed that the phosphorylation levels of SMAD2 were similar in the furin deficient DLD1/*KRAS* and HCA7/WT compared with their corresponding control cells. In contrast, HT29/*BRAF* cells with repressed furin showed significantly decreased levels of phosphorylated SMAD2. These data indicated that furin repression differently affects the activation of SMAD2 in *KRAS*- or *BRAF*-mutated cells.

We then assessed the effect of furin knockout on the expression of NOTCH1 downstream effectors, namely hairy and enhancer of split-1 and -6 (*HES1*, *HES6*), and the hairy/enhancer of split related to YRPW motif protein 1 (*HEY1*) (Fig. 3f). *HES1* was not downregulated despite the slightly impaired processing of NOTCH1. In contrast, *HES6* was significantly downregulated in both DLD1/*KRAS* KO and HT29/*BRAF* KO cells but not in HCA7/KO cells. Analysis of RNA-seq data of primary CRC derived from 275 cases of colonic adenocarcinomas and 92 cases of rectal adenocarcinomas deposited in TCGA database (Fig. 3g–i) [17], revealed that while *HES1* only showed a slight trend of increase, *HES6* is significantly increased. These data suggest that *HES6* is a more important contributor than *HES1* in CRC cells, and that the downregulation of *HES6* might contribute to inhibiting tumorigenic properties in these cells. *HEY1* expression was only upregulated in HCA7/WT KO cells, consistent with the increased NICD levels in these cells. No differences were observed in DLD1/*KRAS* and HT29/*BRAF* cells. *HEY1* expression in the TCGA data set showed a trend towards lower expression in tumor tissue compared with normal tissue, indicating that the upregulation of *HEY1* may contribute to repression of CRC. These results indicate that furin inactivation in colon cancer with mutated *KRAS* or *BRAF* attenuates not only the activation of various furin substrates but also their effectors involved in colon cancer malignant phenotype.

Knockout of furin inhibits the malignant phenotypes of CRC cells with mutated *KRAS* or *BRAF*

We subsequently investigated whether furin inactivation could affect the proliferation rates of colon cancer cells. Both DLD1/*KRAS* and HT29/*BRAF* control cells proliferated faster than HCA7/WT cells (~14- and sevenfold vs. fourfold increase after 7 days, respectively) (Fig. 4a), confirming that *KRAS* or *BRAF* mutations enhance proliferation abilities in colon cancer cells [23, 24]. The inactivation of furin in these cells significantly inhibited cell growth in DLD1/*KRAS* and HT29/*BRAF* cells. In contrast, inactivation of furin in HCA7/WT cells significantly induced their proliferation (Fig. 4a). Similarly, while colony formation assays showed significantly reduced colony number in DLD1/*KRAS* and HT29/*BRAF* cells, increased colony numbers were observed in HCA7/WT cells (Fig. 4b). HCA7/WT control cells formed lower colonies number (±30 colonies/image) than DLD1/*KRAS* (±50 colonies/image) and HT29/*BRAF* (±70 colonies/image) control cells (Fig. 4b), indicating that *KRAS* or *BRAF* activating mutations lead to stronger cellular transformation [25, 26]. These results indicate that the absence of furin mainly influenced the number of colonies in DLD1/*KRAS* cells, whereas it inhibited both the number and size of colonies in HT29/*BRAF* cells. We next analyzed the effect of furin disruption on migration ability of colon cancer cells with mutated *KRAS* or *BRAF* using wound healing assay (Fig. 4c). All

UNCORRECTED PROOF

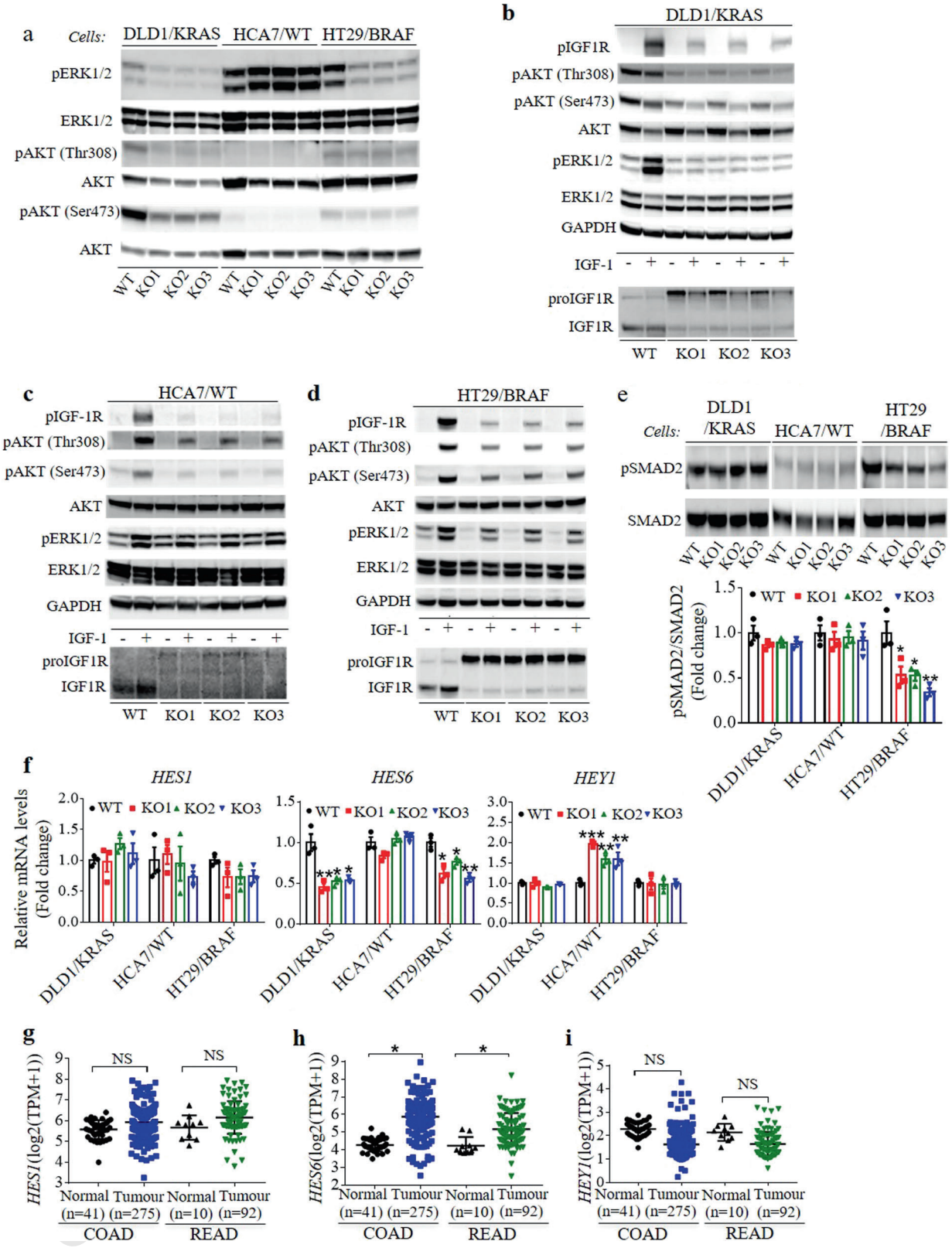

DLD1/*KRAS* KO and HT29/*BRAF* KO cells showed a reduced migration rate compared with control cells after 48 h. The opposite result was obtained with HCA7/WT KO cells.

◀ **Fig. 3 Inactivation of furin reduces ERK/MAPK signaling pathways and regulates the expression of downstream effectors in *KRAS* or *BRAF* mutant CRC cells. a** Immunoblotting of WT cell lysates and furin KO clones of DLD1, HCA7, and HT29 cells. Representative images of autophosphorylation levels of ERK and AKT (Thr308 and Ser473) as well as total AKT and ERK are shown. Immunoblot analysis of IGF1R signaling output in WT cells and furin KO clones of DLD1 (**b**), HCA7 (**c**), and HT29 (**d**) cells. Cells were stimulated by exogenous IGF1 (100 ng/ml, 20 min), and both phosphorylation and total levels of IGF1R, AKT (Thr308 and Ser473), and ERK were checked. The results are representative for three independent experiments. **e** Immunoblot analysis of phosphorylation and total levels of SMAD2 in WT cells and furin KO clones of DLD1, HCA7, and HT29 cells (upper panel), and quantitation of band intensity (lower panel). The mean ± SEM of three independent experiments is shown. **f** qRT-PCR analysis of NOTCH1 downstream targets *HES1*, *HES6*, and *HEY1* in the three CRC WT cells and furin KO clones. The mean ± SEM of three independent experiments is shown. Expression levels of *HES1* (**g**), *HES6* (**h**), and *HEY1* (**i**) in human colorectal adenocarcinomas (COAD + READ) and normal colon and rectal tissue. Expression data are from the TCGA database. Individual data points and means ± SD are provided. COAD colon adenocarcinoma, READ rectum adenocarcinoma, TPM transcripts per million. NS no significant differences. A one-way ANOVA followed by Dunnett's post hoc test was performed for **e** and **f**; A two-tailed Student's *t* test was performed for **j**–**i**. $^{*}P < 0.05$, $^{**}P < 0.01$, $^{***}P < 0.001$.

To evaluate the effect of unprocessed furin substrates on their ability to mediate paracrine effects, we co-cultured colon cancer cells lacking furin with normal fibroblast cells (NFs) and analyzed NFs activation. Indeed, various furin substrates released by colon cancer cells, including TGF-β1, PDGF or VEGF [27] are involved in the activation of stromal fibroblasts into cancer associated fibroblasts (CAFs), which in turn sustains cancer cell migration and invasion [28]. Therefore, we analyzed whether the two CAF-specific markers, α-smooth muscle actin (*ACTA2*) and hypoxia inducible factor 1 alpha (*HIF1A*), were altered in NF-tumor cell co-culturing systems. We found that both *ACTA2* and *HIF1A* underwent significant upregulation when NFs were co-cultured with control colon cancer cells for 3 days (Fig. 4d, e), indicating that colon cancer cell-derived molecules contributed to inducing NFs into CAFs. This upregulation was significantly reduced when NFs were co-cultured with colon cancer lacking furin activity in all three cell lines. These results indicate that reduced levels of mature furin substrate in CRC cells attenuated induction of CAFs from NFs independent of *KRAS* or *BRAF* mutation status.

Furin inactivation has unique effects on gene expression in the different CRC cells

To further investigate the effect of furin inactivation on the malignant phenotype of colon cancer cells with *KRAS* or *BRAF* mutations, we evaluated gene expression in control cells and furin KO cells using RNA-sequencing analysis. Considering genes with at least a twofold change in expression, we found that about 1.8% (423 genes) and 1.1% (263 genes) of the detected transcriptome were affected in the *KRAS*- and *BRAF*-mutated cells DLD1 and HT29, respectively, whereas about 3.8% (879 genes) was deregulated in HCA7 cells (Fig. 5a). Strikingly, most genes were only affected in one cell line, consistent with the enormous heterogeneity of CRCs. Further analysis revealed that only six genes were affected in all three CRC cell types. All of these genes, with the exception of furin, showed different deregulation in the three cell lines (Fig. 5b). Interestingly, we found that four of these genes, *STEAP1*, *PADI1*, *PTGS2*, and *IGFL4* were upregulated in HCA7/WT KO cells but downregulated in DLD1/*KRAS* KO and HT29/*BRAF* KO cells. *PTGS2*, an enzyme involved in the production of prostaglandin E2, is involved in activating the MAPK pathway and in modulating motility, proliferation and resistance to apoptosis in cancer cells [29, 30]. Therefore, we further analyzed the RNA-seq data by qRT-PCR analysis (Fig. 5c) and confirmed that *PTGS2* expression levels decreased in all *KRAS*- or *BRAF*-mutated cells after furin inactivation but not in HCA7/WT cells. TCGA database analysis revealed that *PTGS2* expression positively correlates with furin expression in *KRAS* or *BRAF* mutant colon cancer cells, while there was no correlation between these genes in CRC cells lacking *KRAS* and *BRAF* mutations (Fig. 5d).We then classified the upregulated and downregulated genes in gene ontology (GO) pathways, to identify the characteristic features of CRC cells with WT and mutated *KRAS* or *BRAF* after furin inactivation. GO enrichment analysis also revealed that upregulated genes were significantly enriched in positive regulation of MAPK cascade only in HCA7/WT KO cells (Fig. 5e), which further explains why inactivation of furin led to the oncogenic phenotypes in vitro in HCA7/WT KO cells. In contrast, downregulated genes showed significant enrichment in different GO terms including regulation of cell adhesion and positive regulation of cell migration (Fig. S3a).Taken together, furin inactivation has different effects on gene expression in the three cell lines, which forms the molecular basis for the observed differences in the malignant phenotypes of the colon cancer cells with mutated *KRAS* or *BRAF* on the one hand and the cell lines WT for *KRAS* and *BRAF* on the other hand.

Furin silencing selectively inhibits *KRAS* or *BRAF* mutant CRC cells xenografts growth in vivo

To corroborate the effect of furin inactivation on the malignant phenotype of colon cancer cells with *KRAS* or *BRAF* mutations, we carried out transplant experiments in a mouse model. Although control cells with *KRAS* or *BRAF*

UNCORRECTED PROOF

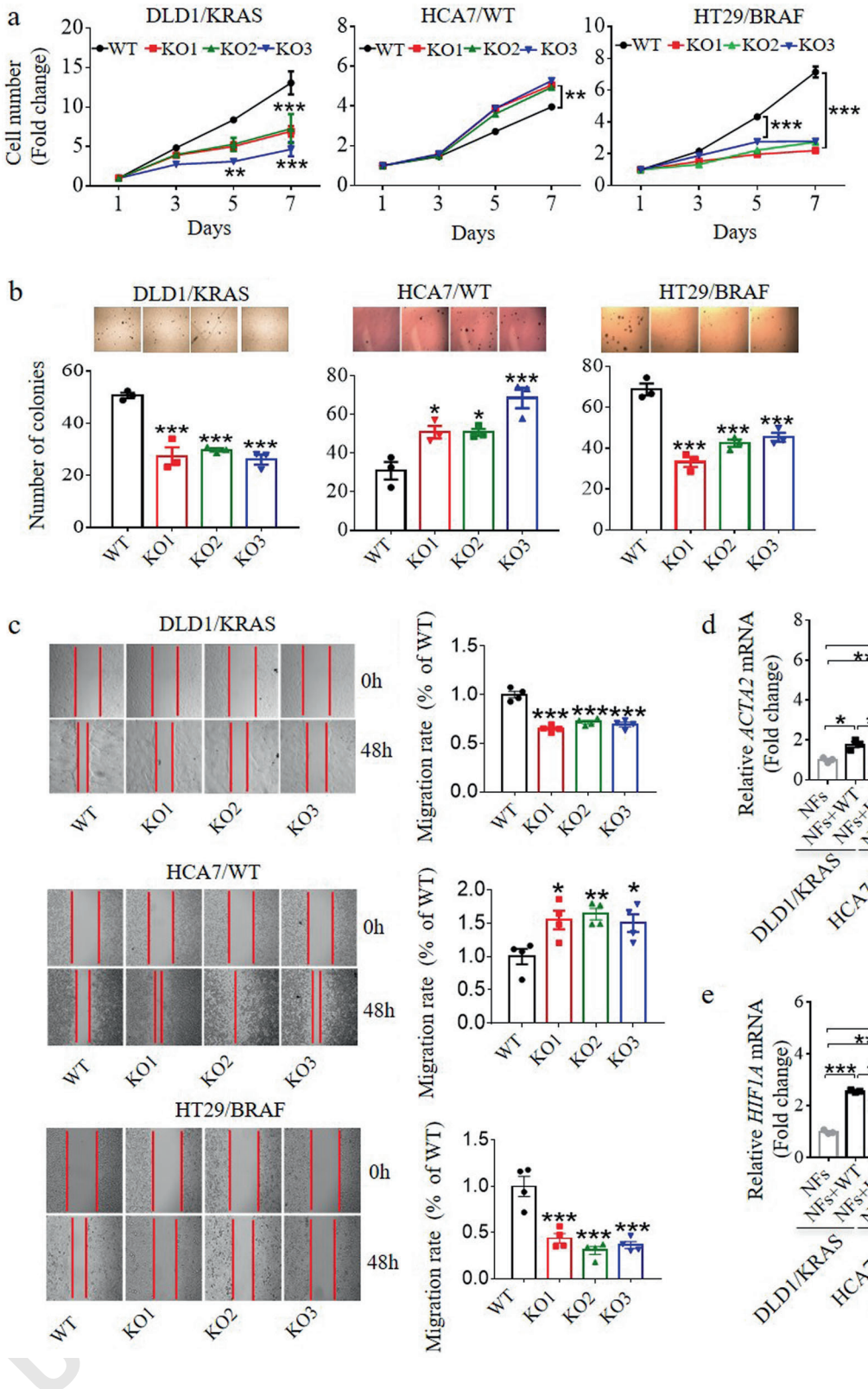

mutations were clearly more aggressive than HCA7/WT, all these colon cancer cells induced tumor formation in immunodeficient mice (Fig. 6a). These data are in line with the in vitro experiments in which cells with *KRAS* or *BRAF* mutation show higher proliferation rates (Fig. 4a). Furin inactivation in these cells significantly reduced tumor growth in vivo, which was also consistent with the effect of furin repression on the proliferation rate in vitro. In contrast,

◀ **Fig. 4 Inactivation of furin inhibits malignant phenotypes of CRC cells with mutated *KRAS* or *BRAF*.** **a** Proliferation curves of WT cells and furin KO clones of DLD1, HCA7, and HT29 cells. The mean ± SEM of three independent experiments is shown. **b** Colony-forming assays for WT and furin KO clones of DLD1, HCA7, and HT29 cells. Representative photos (upper panel) and quantitation of the number of colonies are shown (lower panel). The mean ± SEM of three independent experiments is shown. **c** Time-lapse cell migration assay of WT cells and furin KO clones of DLD1, HCA7, and HT29 cells (left panel). Gap making at 0 h (upper), gap closures relative to closure of initial gap at 48 h (lower), quantitation of migration assays for each CRC cell lines (right panel). The mean ± SEM of four independent experiments is shown. qRT-PCR analysis of *ACTA2* (**d**) and *HIF1A* (**e**) in normal fibroblasts (NFs) without co-culturing tumors (NFs) or co-culturing WT cells (NFs + WT) or furin KO clones (NFs + KO) of DLD1, HCA7, and HT29 cells. The mean ± SEM of three independent experiments is shown. A two-way ANOVA followed by Dunnett's post hoc test was performed for a; a one-way ANOVA followed by Dunnett's post hoc test was performed for **b** and **c**; a two-tailed Student's *t* test was performed for **d** and **e**. $^{*}P < 0.05$, $^{**}P < 0.01$, $^{***}P < 0.001$.

HCA7/WT KO cells did not show clear differences compared with control cells. Although HCA7/WT KO cells had a more aggressive phenotype in vitro, these cells failed to mediate such phenotype in vivo, possibly due to reduced paracrine signaling as shown earlier (Fig. 4d, e). Immunohistochemistry analysis revealed HCA7/WT KO xenografts showed reduced angiogenesis compared with control HCA7/WT xenografts as indicated by the endothelial cell marker CD31 staining. This was also the case in xenografts of DLD/*KRAS* KO and HT29/*BRAF* KO cells (Fig. 6b). This could be the consequence of impaired processing of other furin substrates like VEGFC or PDGF required for tumor angiogenesis [31, 32]. In addition, we observed that HCA7/WT KO and HT29/*BRAF* KO xenografts had more cleaved Caspase-3 staining than control xenografts. Caspase-3 staining in DLD1/*KRAS* KO xenografts was not significantly increased. These results demonstrate that the inactivation of furin in colon cancer cells with mutated *KRAS* or *BRAF* reduces their ability to mediate tumor growth in vivo. Inhibited tumor angiogenesis and enhanced apoptosis are contributing factors.

Discussion

Here we demonstrate that targeting furin impairs the malignant phenotype of the two well-characterized colon cancer cell lines with activating *KRAS* or *BRAF* mutations, DLD1, and HT29, respectively. We show that furin inactivation in these cells reduced their proliferation, migration, and colony formation in vitro and tumor growth and angiogenesis in vivo. Mechanistically, this is achieved by inhibition of the endoproteolytic cleavage and hence activation of various furin substrates which are oncogenic drivers in CRC, including IGF1R, IR, TGF-β1, NOTCH1, and c-MET. Altogether, this resulted in a robust downregulation of the MAPK signaling pathway in DLD1/*KRAS* KO and HT29/*BRAF* KO but not HCA7/WT KO cells. RNA-seq analysis allowed us to identify various genes differentially regulated in the furin KO cells dependent on *KRAS* or *BRAF* mutation status. One such gene is *PTGS2*, which is involved in activating the MAPK pathway [30]. *PTGS2* is downregulated in DLD1/*KRAS* KO and HT29/*BRAF* KO cells but upregulated in HCA7/WT KO cells.

Receptor tyrosine kinases (RTKs), as essential components of MAPK, have become most important targets in CRC treatment. However, there is increasing evidence that crosstalk between different RTKs render CRC cells resistant to single RTK inhibitor treatment. For example, amplification of *c-MET* in tumor cells results in acquired resistance to anti-EGFR therapy in CRC patients, which could be overcome with a combination of a c-MET inhibitor and a EGFR inhibitor [20]. Thus, targeting different RTKs simultaneously is likely to improve treatment efficacy of single target RTK inhibitors. IR, IGF1R, and c-MET have been explored as potential therapeutic targets in CRC. Like other RTK inhibitors, targeting these RTKs alone led to acquired resistance due to crosstalk [33, 34]. Also, mutations in RTK downstream effectors like KRAS and BRAF led to unresponsive RTK inhibitors. Unlike these available inhibitors, inactivation of furin simultaneously inhibited activation of IR, IGF1R, and c-MET. Moreover, the ligands of IGF1R like IGF1 and IGF2 are also activated by furin cleavage [35, 36]. Inactivation of furin produced robust inhibition in downstream pathways of RTKs including the ERK/MAPK and PI3K/AKT pathways in DLD1 and HT29 cells harboring *KRAS* or *BRAF* mutations, respectively. Therefore, inhibition of furin could be an alternative therapeutic approach to inhibit mutant *KRAS* or *BRAF* CRC cells by inhibiting multiple RTKs and their ligands.

Unexpectedly, HCA7/WT KO clones showed a slight increase in the activity of ERK/MAPK pathway. Although we did not find the upregulation of other RTK members including *EGFR*, *ERBB2*, and *ERBB3* in HCA7/WT KO cells, RNA-seq data revealed that the inactivation of furin in HCA7 cells led to the upregulation of multiple genes like *PTGS2* which positively regulate multiple oncogenic pathways including the MAPK cascade. Direct overexpression of recombinant *PTGS2* in CRC cells enhanced its tumorigenic properties, and this phenotype could be reversed via PTGS2 inhibitor [37]. Similarly, induction of *PTGS2* led to an aggressive phenotype in CRC cells [38]. In contrast, inhibition of *PTGS2* via aspirin significantly inhibited tumorigenic properties in a wide array of CRC cells [39]. Thus, *PTGS2* has an important role in colorectal carcinogenesis and upregulated *PTGS2* could activate the ERK/MAPK pathway. Furthermore, it was recently reported that

UNCORRECTED PROOF

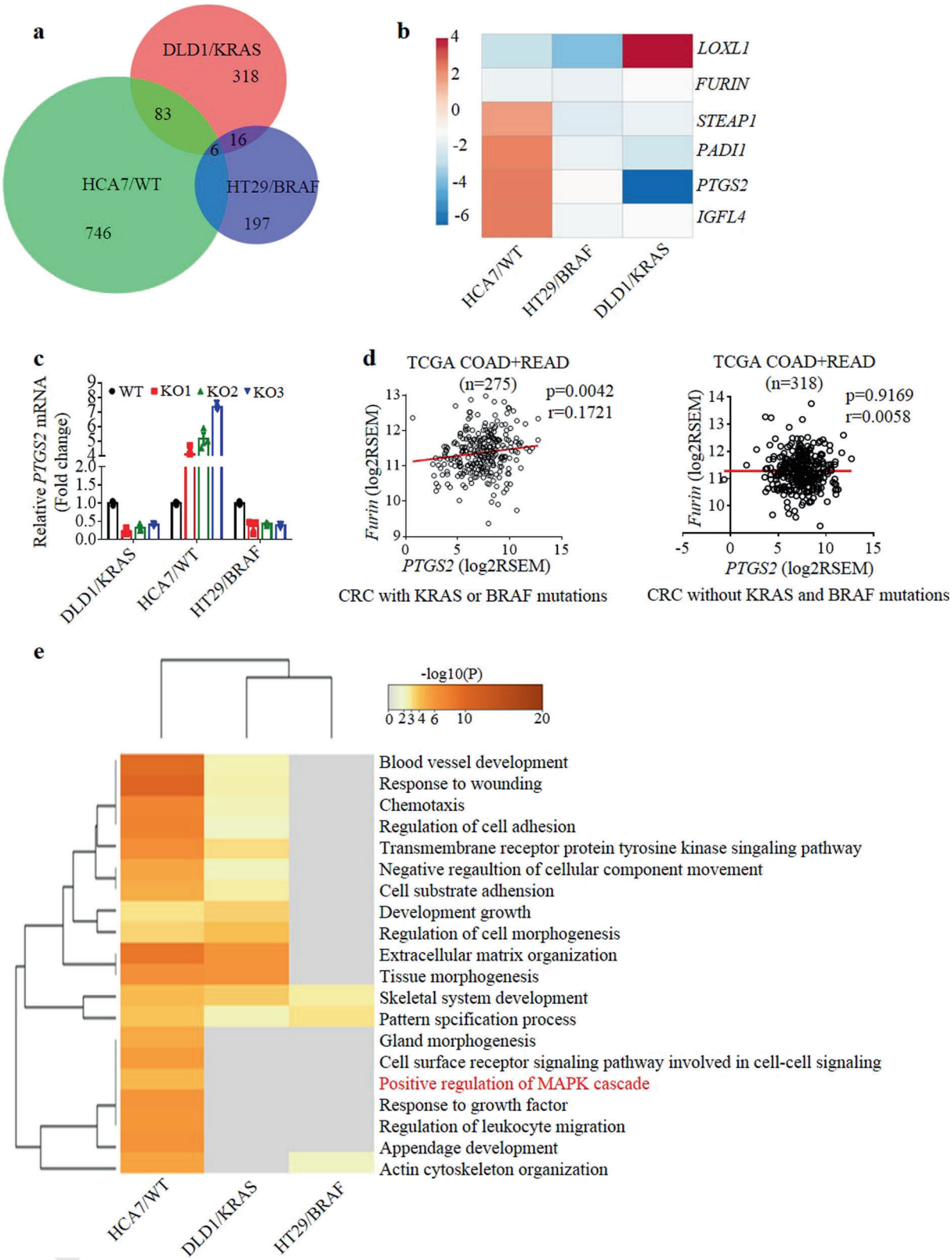

the expression level of IGF1R was higher in CRC with *KRAS* or *BRAF* mutations than in those without [40]. Our findings also showed that HCA7/WT cells have lower expression of IGF1R and c-MET than DLD1/*KRAS* and HT29/*BRAF* cells (Fig. 2c and g). Since these substrates have the different contributions to colorectal carcinogenesis,

Fig. 5 Inactivation of furin causes distinct changes in gene expression of different CRC cells. a Venn diagram of genes with significant ($P < 0.05$) differential expression and two or more fold change in WT or furin KO clones of DLD1, HCA7, and HT29 cells. Data are derived from two biological replicates. **b** Heat map showing the relative log2 fold change of the six genes commonly affected by disruption of furin in DLD1, HCA7, and HT29 cells, as shown in the Venn diagram. **c** Relative *PTGS2* mRNA levels in WT cells and three furin KO clones of DLD1, HCA7, and HT29 cells. The mean ± SEM of three independent experiments is shown. **d** Correlation of furin expression with PTGS2 expression in primary colorectal tumors with *KRAS* or *BRAF* mutations ($n = 275$) or without *KRAS* or *BRAF* mutations ($n = 318$). Expression data are from the TCGA collection of human colorectal adenocarcinomas. Each dot represents one sample. The strength of the correlation was determined using the Spearman's correlation coefficient (r), and the two-tailed P value was calculated. A linear regression-fitting curve is shown as a dotted red line. RSEM: RNA-Seq by Expectation Maximization. **e** Heat map representing top 20 enriched gene ontology biological processes among upregulated genes caused by loss of furin in DLD1, HCA7, and HT29 cells. Positive regulation of MAPK cascade was significantly enriched only in HCA7 KO clones. The colors represent statistical significance ($-\log10(P$ value)).

their distinct expression levels may explain the discrepancy of phenotypes in furin KO CRC cells with or without *KRAS*/*BRAF* mutations. It would not be surprising that the contribution of downregulated IGF1R and c-MET expression/activity to inhibition of the MAPK pathway could be reduced or even reversed by increased expression of *PTGS2* in HCA/WT KO cells. Accordingly, in previous studies, we found that inhibition of furin increased ERK activation in T cells, which have WT *KRAS* and *BRAF* [41]. Overall, the upregulation of MAPK cascade and *PTGS2* expression could partially explain why furin deficiency causes aggressive phenotypes in HCA7/WT KO cells or in hepatocellular carcinoma with WT *KRAS* and *BRAF* [42, 43].

Low *PTGS2* expression has been associated with better survival in colorectal adenocarcinoma patients with *KRAS*- or *BRAF*-mutated tumors, but not in patients with WT *KRAS* and *BRAF* [44, 45]. Our study also identified that *furin* expression positively correlated with *PTGS2* expression only in CRC patients with *KRAS* or *BRAF* mutant tumor (Fig. 5d). In addition, we found that furin deficiency led to the upregulation of *PTGS2* expression in HCA7/WT KO cells (Fig. 5b). This is consistent with the finding that furin deficiency resulted in increased expression in *PTGS2* in immune cells that has WT *KRAS* and *BRAF* [46]. However, the underlying mechanisms how furin regulates *PTGS2* expression in the context of *KRAS* or *BRAF* mutations remains unclear.

Furin inactivation also reduced NOTCH1 processing into NICD in DLD1 and HT29 furin KO clones, while NICD levels were upregulated in HCA7 furin KO clones. This upregulation might have contributed to the upregulation of the MAPK activity in HCA7 furin KO clones since NICD activates MAPK cascade via *KRAS* [47]. In HCA7 cells, upregulation of NICD could activate WT *KRAS* which further activates ERK.

Inactivation of furin also inhibited activation of TGF-β1 which plays an important role in CRC, especially in late stages due to its paracrine effects or its immunosuppressive role in tumor microenvironment [48]. Since these CRC cells have an inactivated TGF-β signaling pathway owing to either *TGFBR2* or *SMAD4* mutations [49], they did not respond to reduced TGF-β1 production. In contrast, the paracrine effect of TGF-β1 was clearly reduced in vitro and in vivo, which contributed to inhibiting aggressive phenotypes in vivo in HCA7/WT KO cells (Fig. 6a).

Furin has many additional substrates that might have contributed to the observed phenotypes. For instance, furin is involved in the processing of the V-ATPase subunit Ac45 [50], which may control micropinocytosis in *KRAS*-driven tumor cells [51]. It would not be surprising that inhibition of furin could suppress tumorigenic properties of pancreatic cancer cells with *KRAS* or *BRAF* mutations by inhibiting other oncogenic pathways [52].These results show that the inactivation of furin provides a synergistic strategy interfering with multiple oncogenic pathways, which can enhance the therapeutic efficacy in CRC treatment.

Currently, no specific small molecule inhibitor of furin has been developed, although several different type of nonspecific furin inhibitors are available [53]. All available inhibitors cross-react to a variable extent, as the substrate binding region of the catalytic domain of furin is highly similar to the other PCs [54]. The most commonly used inhibitors, hexa-D-arginine and Decanoyl-Arg-Val-Lys-Arg-chloromethylketone, are highly potent, but also inhibit other PCs [55, 56]. The inhibition of multiple PCs is likely to increase side effects. A recently developed inhibitor, MI-1148 (4-guanidinomethyl-phenylacteyl-Arg-Tle-Arg-4-amidinobenzylamide) shows strong inhibition of furin [57], but was also shown to inhibit PC1/3 and to a lesser extent PC2. Furthermore, MI-1148 also inhibits other types of serine proteases like thrombin and matriptase [58]. This emphasizes the need to develop furin-specific inhibitors. Proof of concept is the furin-inhibiting nanobodies that bind non-competitively to furin and inhibit its activity by steric exclusion [59]. Besides pharmacological inhibitors, genetically inhibited furin via shRNA in tumor cells is also promising strategy to inhibit furin in a specific manner. For instance, an autologous cancer cell vaccine against furin has been tested in cancer patients [60].

In this study we have focused on *KRAS* or *BRAF* mutations in two well-characterized CRC cell lines. Therefore, it remains to be established what the effect of furin inactivation in a clinical setting would be. Also, the side effects of prolonged furin inhibition are unknown, although short-term inhibition using hexa-D-arginine is non-cytotoxic in vivo [61]. However, the insights from this study clearly indicate that furin inhibition is a novel strategy

UNCORRECTED PROOF

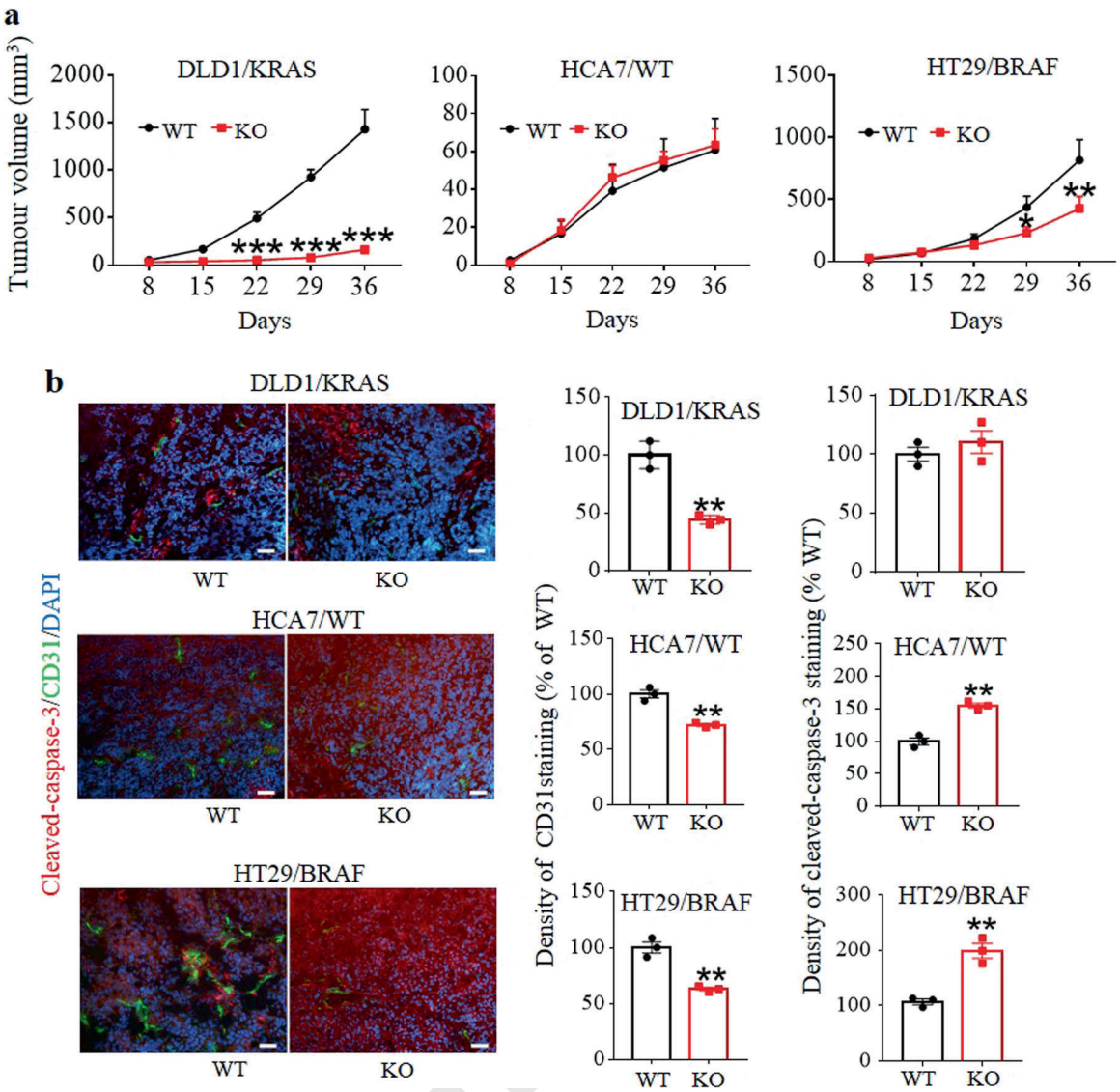

Fig. 6 Furin deficiency selectively inhibits *KRAS* or *BRAF* mutant CRC cells xenografts growth in vivo. a Growth curves of tumor xenografts in nude mice for each CRC cell line. Tumor growth is expressed as its volumes. $n = 5$ mice per group. **b** Tumor tissue from CRC xenografts were evaluated by immunofluorescence (IF) for a marker for cell apoptosis (cleaved caspase-3; red signal) and a marker of angiogenesis (CD31; green signal). Representative images of tumor cell apoptosis and angiogenesis in CRC xenografts are shown in the left panels. Scale bar: 50 µm. Quantitation of density of cleaved caspase-3 and CD31 in CRC xenografts are shown in the right panels. Bar graphs indicate the relative density compared with WT CRC xenografts. The mean ± SEM is shown. A two-way ANOVA followed by Dunnett's post hoc test was performed for **a**; a two-tailed Student's *t* test was performed for **b**. $^{*}P < 0.05$, $^{**}P < 0.01$, $^{***}P < 0.001$.

to simultaneously inhibit multiple oncogenic proproteins in CRC cells with *KRAS* or *BRAF* mutations.

Materials and methods

Human tumor samples

Freshly resected colon tumor tissues and their non-cancerous counterparts were obtained from Bergonié Institute, Bordeaux, France. All specimens were obtained following written informed consent approved by Bergonié Institute. Biopsies were de-identified and samples were processed histology studies.

Cell lines

HEK-293T and the human CRC cell lines DLD1, HCA7, and HT29 were obtained from the American Type Culture Collection. Normal human dermal fibroblasts were from G. Matthijs (KU Leuven, Leuven, Belgium) [62]. They were maintained in culture for no more than 15 continuous passages. HEK-293T cells and normal human dermal fibroblasts were cultured in DMEM/F12 medium supplemented

UNCORRECTED

with 10% fetal calf serum (FCS, Perbio Science). DLD1 and HCA7 cell lines were maintained in DMEM/F12 medium supplemented with 10% heat-inactivated FCS and 1% penicillin–streptomycin (Life Technologies); HT29 cell line was maintained in McCoy's 5A (Modified) medium supplemented with 10% heat-inactivated FCS and 1% penicillin–streptomycin (Life Technologies). All cell lines tested negative for mycoplasma.

CRISPR-Cas9-based furin knockout

The 20-nt single guide RNA targeting the exon 2 of human furin (Fig. 2a) was designed using the CRISPR design tool [63]. The sgRNA sequence, 5′-GAAGGTCTTCACCAAC ACGT-3′, was cloned into BsmBI-digested lentiCRISPR v2 (Addgene). In order to produce lentivirus, HEK-293T cells were resuspended in DMEM medium and cotransfected with 8 µg of gRNA expression constructs, 6 µg psPAX2 vector (Addgene), and 4 µg pVSVG (Addgene) vector in 40 µL of Lipofectamine 2000 (Invitrogen) in Opti-MEM medium. The medium was aspirated after 6 h and replaced with fresh DMEM/F12 with 10% FCS. The supernatant was harvested after 48 h, centrifuged at 1000 g at 4 °C for 10 min, filtered through a 0.45 µm low protein-binding membrane (Millipore), and used to infect CRC cells in the presence of 8 mg/ml polybrene (Sigma). The virus-containing media were removed 48 h after transduction, and infected cells were selected with puromycin (2 µg/ml). Furin KO clones were selected using serial dilutions and expanded. The expression of furin was evaluated by an immunoblotting assay and confirmed by Sanger sequencing.

Cell proliferation assay

Cell viability was determined using a WST-1 cell proliferation assay according to the manufacturer's protocol (Roche). Briefly, cells were counted and plated at a density of 2 × 103 cells/well in 96-well plates in triplicates and cultured at 37 °C with 5% CO2 in a humidified atmosphere. WST-1 reagent was added at 1, 3, 5, or 7 days, and incubation was continued for an additional 3 h. Spectrophotometry was measured using a microplate reader at a wavelength of 450 nm (PerkinElmer, VICTOR™ X3).

Soft agar assay

Cells (1×10^4 cells/well) were suspended in a top layer of 0.4% agar (Becton Dickinson) in DMEM/F12 or McCoy's 5A (Modified) medium containing 2 µg/µl Fungizone (Life Technology), and then plated on a bottom layer of 0.6% agar in related medium supplemented with 2 µg/µl Fungizone in six-well plates. Cells were re-fed with medium every 3 days. After 14 days, the medium was discarded, and cells were washed twice with PBS. Colonies were stained with 0.05% crystal violet (Sigma) for 1 h. Excess of staining solution was carefully removed with PBS, and then colonies were counted using Image J from three independent dishes of each group.

Wound healing migration assay

Cells were plated at a density of 5×10^4 cells/well in 12-well plates in an attached silicone insert with a defined cell-free gap (Ibidi) for 12–24 h to reach 80% of confluence. The wound was created by removing inserts from 12-well plate. Medium was refreshed to remove dead cells and the cells were observed under an inverted light microscope. The images were taken using a light microscope (×5 magnification) fitted with a microscope camera (Olympus IX71) at time intervals of 0 and 48 h. Cell migration towards the wound was expressed as a percentage of wound closure: percentage of wound closure = [(D0 − DT=)/D0] × 100% where, D0 is the area of wound measured immediately after the wound was made, and DT is the area of wound measured 48 h after the wound was made.

Co-culture of fibroblasts and tumor cells

NFs and tumor cells were plated in 12-well plates at 1×10^5 cells/well and on the inserts for 12-well plates (VWR International) at 5×10^4 cells/insert, respectively. Tumor cells and fibroblasts were then starved for 24 h. Afterwards, inserts with or without tumor cells were transferred into wells with fibroblasts in 12-well plate. After co-culturing for 72 h, fibroblasts were harvested for RNA isolation.

Immunoblotting

Cells were lysed in cell lysis buffer (Cell Signaling Technology) with EDTA-free protease inhibitor cocktail and phosphatase inhibitors (Roche). After brief sonication, the preparation was centrifuged, and the supernatants were used as cell lysates. For the phosphorylation assay, cells were maintained in serum-free medium overnight, and then incubated with recombinant human IGF1 protein (100 ng/ml, Abcam) for 20 min or recombinant human insulin protein (100 ng/ml, Actrapid) for 20 min. After that, cells were harvested in lysis buffer. The protein concentration was measured using a Pierce™ BCA protein assays kit (Thermo Fisher Scientific). For TGF-β1, conditioned medium without serum was collected after 48 h and then 1 volume of 100% trichloroacetic acid (Sigma) was added to 4 volumes of the medium. The proteins were precipitated overnight at 4 °C and washed twice with −20 °C acetone (Thermo Fisher Scientific). The samples were dried and resuspended

UNCORRECTED PROOF

in 1× SDS loading buffer (Cell Signaling Technology) prior to immunoblotting analysis. Proteins were resolved on 10% precast or 4–12% gradient gels (Invitrogen) and transferred to a nitrocellulose membrane. After blocking with 5% non-fat milk in Tris-buffered saline with 0.2% Triton X-100, membranes were incubated with the primary antibody followed by the secondary antibody conjugated with horseradish peroxidase. After washing, the bands were visualized with enhanced chemiluminescence substrate (Perkin Elmer) and quantified using Image Quant LAS4000 (GE Healthcare). Membranes were re-probed with a blot restore solution following manufacturer's instructions (Thermo Fisher Scientific). Detailed information on the antibodies used is given in supplementary data (Supplementary Table S1).

Quantitative RT-PCR

For gene expression analysis, total RNA from cultured cells were isolated using the NucleoSpin® RNA kit (Macherey-Nagel) according to the manufacturer's protocol. Reverse transcription of the RNA was performed using random primers iScript™ cDNA Synthesis Kit (Bio-Rad). Real-time PCR and data collection were performed with IQ SYBR Green supermix reagent (Bio-Rad) on a CFX connect instrument (Bio-Rad). Each sample was run in triplicate and normalized to the housekeeping gene *GAPDH*. Relative fold changes in gene expression were calculated using the ΔCT method with the equation 2ΔΔCT. The results are shown as fold changes compared with the control group average or relative levels to *GAPDH*. See supplementary data (Supplementary Table S2) for primer sequences.

Immunofluorescence assay

Human colon cancer and its corresponding non-cancer colon tissues were cut into smaller pieces and snap-frozen in liquid nitrogen until use. Frozen pieces were embedded in OCT (Sakura) prior to sectioning on a microtome-cryostat (Leica CM1900) at 10-µM thickness. Sections were mounted in gelatin-coated slides and stored at −20 °C. For immunohistochemistry, tumor samples were fixed in 2% paraformaldehyde for 10 min and cryopreserved in 30% sucrose solution. The samples were embedded in OCT to produce frozen blocks and stored at −80 °C. Sections were incubated in the primary antibodies diluted 1:100 in PBS-0.1% BSA, overnight at 4 °C. For furin detection, anti-furin (H-220; B6) were obtained from Santa Cruz Biotech. The sections were incubated with the appropriate fluorophore-conjugated secondary antibody at 1:500 (Fluoprobes and Interchim) for 1 h at room temperature and sections were mounted with ProLong Gold Antifade mounting medium containing DAPI (Invitrogen). For mouse tumor analysis, frozen tumor sections were blocked with 5% milk in PBS containing 0.5% Triton X-100 and were stained with unconjugated primary antibodies CD31 (Cell Signaling Technology) and cleaved caspase-3 (Millipore) for 15 min at 4 °C, the washed twice with PBS before incubation with fluorochrome-associated secondary antibodies. All samples were mounted with proLong containing DAPI (Invitrogen) and confocal immunofluorescence images were taken using the inverted Nikon C2si Eclipse Ti-S microscope with NIS-Elements AR software (Nikon Instruments Europe B.V.)

In vivo tumorigenic assay

Mice were housed in ventilated carousel racks and provided with sterile food and drinking water. Approximately 1×10^6 tumor cells were injected subcutaneously into the midline of the back of 6–8-week-old immunodeficient *RAG2*−/−γc−/− mice. Tumor size was evaluated once or twice weekly by caliper measurements and approximate volume of the mass was calculated using the formula length × (width)^2 × 0.5. Animals were randomized into groups. Data points were expressed as an average tumor volume. All in vivo experiments were approved by the Animal Housing and Experiment Board of the University of Bordeaux and performed in compliance with the French guidelines for experimental animal studies.

RNA-seq and enrichment analysis

Furin WT and furin KO cell samples of the three CRC cell lines were subjected to mRNA sequencing at Leuven Genomics Core Facility. Briefly, 1 µg of total RNA was used as input for the Illumina TruSeq RNA sample prep kit (Illumina). Final libraries were quantified using the Qubit High Sensitivity assay (Life Technologies). Sequencing was done on an Illumina HiSeq. 2500 using the 51 bp. For RNA-Seq data analysis, splice-aware alignment was performed with TopHat against the human hg19. Quantification of reads per gene was performed with HT-Seq count. Count-based differential expression analysis was carried out with R-based Bioconductor package DESeq. Reported *p* values were adjusted for multiple testing with the Benjamini-Hochberg procedure, which controls false discovery rate (FDR). Genes with a fold change of >2 (both up and down) and FDR < 0.05 were selected for GO biological processes by the metascape online tool (http://metascape.org) [64]. All genes in the human genome were used as the enrichment background. Terms with $P < 0.01$, minimum overlap 3, and enrichment factor > 1.5 were selected for analysis. A detailed list of all terms and results for each analysis are provided in the supplementary data (Supplementary dataset 1 and dataset 2). RNA-seq expression data have been deposited at the Gene Expression Omnibus, under accession number GSE130969. TCGA RNA-seq data were obtained from the cBioPortal database [65].

UNCORRECTED PROOF

Statistics

Data are presented as mean ± SEM, unless otherwise indicated. For all data, when comparing two groups, a two-tailed unpaired Student's *t* test was conducted. For three or more groups, the statistical significance was analyzed using one-way or two-way ANOVA followed by Dunnett's post hoc test. The strength of association between two variables and the direction of the relationship was explored with non-parametric correlation coefficient analysis (spearman), and the two-tailed *P* value was calculated. Data distribution was examined for normality by visual observation of the variation of data points within experimental groups. $P < 0.05$ was considered statistically significant. Statistics were calculated with Prism (GraphPad 7).

Data availability

All raw RNA-sequencing data can be found at the NCBI Gene Expression Omnibus (accession number: GSE130969). Raw data for figures are available as source data to the relevant figure. All other datasets generated and analyzed during the current study are available from the corresponding authors upon reasonable request. Any requests for data or materials should be addressed to JC.

Acknowledgements We would like to thank Maria Francesca Baietti for providing help with the soft agar assay, and Rudra Kashyap for providing help with the wound healing migration assay. We would also like to thank Álvaro Cortés Calabuig for the RNA-seq data analysis. This work was supported in part by SIRIC BRIO and La Ligue Contre le Cancer to AMK, France. We acknowledge grant support from FWO Vlaanderen (Grant nr. G.0738.15) to JC. ZH was supported by a Chinese Government Scholarship (Nr. 201409110101).

Author contributions ZH and JC designed the research. ST provided advice on the research. SE provided human samples. ZH performed the majority of in vitro experiments. GS and AMK performed the in vivo tumorigenic assay and immunofluorescence assay. ZH and LT performed bioinformatics analysis of RNA-seq data. SM performed cell culture. ZH collected and analyzed the data and wrote the manuscript with input from JC, AMK, and GS. AMK and JC supervised the research.

Compliance with ethical standards

Conflict of interest The authors declare that they have no conflict of interest.

Publisher's note Springer Nature remains neutral with regard to jurisdictional claims in published maps and institutional affiliations.

References

1. Bray F, Ferlay J, Soerjomataram I, Siegel RL, Torre LA, Jemal A. Global cancer statistics 2018: GLOBOCAN estimates of incidence and mortality worldwide for 36 cancers in 185 countries. CA Cancer J Clin. 2018;68:394–424.
2. Sanchez-Vega F, Mina M, Armenia J, Chatila WK, Luna A, La KC, et al. Oncogenic signaling pathways in the cancer genome atlas. Cell. 2018;173:321–37.
3. Muzny DM, Bainbridge MN, Chang K, Dinh HH, Drummond JA, Fowler G, et al. Comprehensive molecular characterization of human colon and rectal cancer. Nature. 2012;487:330–7.
4. Van Cutsem E, Köhne C-H, Hitre E, Zaluski J, Chang Chien C-R, Makhson A, et al. Cetuximab and chemotherapy as initial treatment for metastatic colorectal cancer. N Engl J Med. 2009;360:1408–17.
5. De Roock W, De Vriendt V, Normanno N, Ciardiello F, Tejpar S. KRAS, BRAF, PIK3CA, and PTEN mutations: implications for targeted therapies in metastatic colorectal cancer. Lancet Oncol. 2011;12:594–603.
6. Creemers JWM, Khatib A-M. Knock-out mouse models of proprotein convertases: unique functions or redundancy? Front Biosci. 2008;13:4960–71.
7. Artenstein AW, Opal SM. Proprotein convertases in health and disease. N Engl J Med. 2011;365:2507–18.
8. Siegfried G, Descarpentrie J, Evrard S, Khatib AM. Proprotein convertases: Key players in inflammation-related malignancies and metastasis. Cancer Lett. 2020;473:50–61.
9. Scamuffa N, Siegfried G, Bontemps Y, Ma L, Basak A, Cherel G, et al. Selective inhibition of proprotein convertases represses the metastatic potential of human colorectal tumor cells. J Clin Investig. 2008;118:352–63.
10. Lopez de Cicco R, Bassi DE, Page R, Klein-Szanto AJ. Furin expression in squamous cell carcinomas of the oral cavity and other sites evaluated by tissue microarray technology. Acta Odontol Latinoam. 2002;15:29–37.
11. Bassi DE, Mahloogi H, Al-Saleem L, De Cicco RL, Ridge JA, Klein-Szanto AJP. Elevated furin expression in aggressive human head and neck tumors and tumor cell lines. Mol Carcinog. 2001;31:224–32.
12. Page RE, Klein-Szanto AJP, Litwin S, Nicolas E, Al-Jumaily R, Alexander P, et al. Increased expression of the pro-protein convertase furin predicts decreased survival in ovarian cancer. Cell Oncol. 2007;29:289–99.
13. Jaaks P, D'Alessandro V, Grob N, Büel S, Hajdin K, Schäfer BW, et al. The proprotein convertase furin contributes to rhabdomyosarcoma malignancy by promoting vascularization, migration and invasion. PLoS ONE. 2016;11:e0161396.
14. Scamuffa N, Sfaxi F, Ma J, Lalou C, Seidah N, Calvo F, et al. Prodomain of the proprotein convertase subtilisin/kexin Furin (ppFurin) protects from tumor progression and metastasis. Carcinogenesis. 2014;35:528–36.
15. Oh J, Barve M, Matthews CM, Koon EC, Heffernan TP, Fine B, et al. Phase II study of Vigil® DNA engineered immunotherapy as maintenance in advanced stage ovarian cancer. Gynecol Oncol. 2016;143:504–10.
16. Khatib A-M, Siegfried G, Prat A, Luis J, Chrétien M, Metrakos P, et al. Inhibition of proprotein convertases is associated with loss of growth and tumorigenicity of HT-29 human colon carcinoma cells. J Biol Chem. 2001;276:30686–93.
17. Tang Z, Li C, Kang B, Gao G, Li C, Zhang Z. GEPIA: a web server for cancer and normal gene expression profiling and interactive analyses. Nucleic Acids Res. 2017;45:W98–W102.
18. Roebroek AJM, Taylor NA, Louagie E, Pauli I, Smeijers L, Snellinx A, et al. Limited redundancy of the proprotein convertase furin in mouse liver. J Biol Chem. 2004;279:53442–50.
19. Kopan R, Ilagan MXG. The canonical notch signaling pathway: unfolding the activation mechanism. Cell. 2009;137:216–33.
20. Bardelli A, Corso S, Bertotti A, Hobor S, Valtorta E, Siravegna G, et al. Amplification of the MET receptor drives resistance to anti-

UNCORRECTED PROOF

EGFR therapies in colorectal cancer. Cancer Discov. 2013;3:658–73.
21. Van Schaeybroeck S, Kalimutho M, Dunne PD, Carson R, Allen W, Jithesh PV, et al. ADAM17-dependent c-MET-STAT3 signaling mediates resistance to MEK inhibitors in KRAS mutant colorectal cancer. Cell Rep. 2014;7:1940–55.
22. Johnson P, Roberts PJ, Der CJ, Benvenuti S, Sartore-Bianchi A, Di Nicolantonio F, et al. Oncogenic activation of the RAS/RAF signaling pathway impairs the response of metastatic colorectal cancers to anti-epidermal growth factor receptor antibody therapies. Oncogene. 2007;26:2643–8.
23. Holderfield M, Deuker MM, McCormick F, McMahon M. Targeting RAF kinases for cancer therapy: BRAF-mutated melanoma and beyond. Nat Rev Cancer. 2014;14:455–67.
24. Liu X, Jakubowski M, Hunt JL. KRAS gene mutation in colorectal cancer is correlated with increased proliferation and spontaneous apoptosis. Am J Clin Pathol. 2011;135:245–52.
25. Vartanian S, Bentley C, Brauer MJ, Li L, Shirasawa S, Sasazuki T, et al. Identification of mutant K-Ras-dependent phenotypes using a panel of isogenic cell lines. J Biol Chem. 2013;288:2403–13.
26. Liu D, Liu Z, Condouris S, Xing MM. BRAF V600E maintains proliferation, transformation, and tumorigenicity of BRAF-mutant papillary thyroid cancer cells. J Clin Endocrinol Metab. 2007;92:2264–71.
27. Zhang D, Wang Y, Shi Z, Liu J, Sun P, Hou X, et al. Metabolic reprogramming of cancer-associated fibroblasts by IDH3α downregulation. Cell Rep. 2015;10:1335–48.
28. Erdogan B, Webb DJ. Cancer-associated fibroblasts modulate growth factor signaling and extracellular matrix remodeling to regulate tumor metastasis. Biochem Soc Trans. 2017;45:229–36.
29. Wang D, Dubois RN. Eicosanoids and cancer. Nat Rev Cancer. 2010;10:181–93.
30. Krysan K, Reckamp KL, Dalwadi H, Sharma S, Rozengurt E, Dohadwala M, et al. Prostaglandin E2 activates mitogen-activated protein kinase/Erk pathway signaling and cell proliferation in non-small cell lung cancer cells in an epidermal growth factor receptor-independent manner. Cancer Res. 2005;65:6275–81.
31. Siegfried G, Basak A, Cromlish JA, Benjannet S, Marcinkiewicz J, Chrétien M. et al. The secretory proprotein convertases furin, PC5, and PC7 activate VEGF-C to induce tumorigenesis. J Clin Investig. 2003;111:1723–32.
32. Siegfried G, Basak A, Prichett-Pejic W, Scamuffa N, Ma L, Benjannet S, et al. Regulation of the stepwise proteolytic cleavage and secretion of PDGF-B by the proprotein convertases. Oncogene. 2005;24:6925–35.
33. Buck E, Gokhale PC, Koujak S, Brown E, Eyzaguirre A, Tao N, et al. Compensatory insulin receptor (IR) activation on inhibition of insulin-like growth factor-1 receptor (IGF-1R): Rationale for cotargeting IGF-1R and IR in cancer. Mol Cancer Ther. 2010;9:2652–64.
34. Ulanet DB, Ludwig DL, Kahn CR, Hanahan D. Insulin receptor functionally enhances multistage tumor progression and conveys intrinsic resistance to IGF-1R targeted therapy. Proc Natl Acad Sci USA. 2010;107:10791–8.
35. Duguay SJ, Milewski WM, Young BD, Nakayama K, Steiner DF. Processing of wild-type and mutant proinsulin-like growth factor-IA by subtilisin-related proprotein convertases. J Biol Chem. 1997;272:6663–70.
36. Duguay SJ, Jin Y, Stein J, Duguay AN, Gardner P, Steiner DF. Post-translational processing of the insulin-like growth factor-2 precursor. Analysis of O-glycosylation and endoproteolysis. J Biol Chem. 1998;273:18443–51.
37. Tsujii M, Kawano S, Dubois RN. Cyclooxygenase-2 expression in human colon cancer cells increases metastatic potential. Proc Natl Acad Sci USA. 1997;94:3336–40.
38. Wang D, Dubois RN. The role of COX-2 in intestinal inflammation and colorectal cancer. Oncogene. 2010;29:781–8.
39. Shimura T, Toden S, Komarova NL, Boland C, Wodarz D, Goel A. A comprehensive in vivo and mathematic modeling-based kinetic characterization for aspirin-induced chemoprevention in colorectal cancer. Carcinogenesis. 2020. https://doi.org/10.1093/carcin/bgz195.
40. Jin M, Long Z-W, Yang J, Lin X. Correlations of IGF-1R and COX-2 expressions with Ras and BRAF genetic mutations, clinicopathological features and prognosis of colorectal cancer patients. Pathol Oncol Res. 2018;24:45–57.
41. Tomé M, Pappalardo A, Soulet F, López JJ, Olaizola J, Leger Y, et al. Inactivation of proprotein convertases in T cells inhibits PD-1 expression and creates a favorable immune microenvironment in colorectal cancer. Cancer Res. 2019;79:5008–21.
42. Declercq J, Brouwers B, Pruniau VPEG, Stijnen P, Tuand K, Meulemans S. et al. Liver-specific inactivation of the proprotein convertase FURIN leads to increased hepatocellular carcinoma growth. Biomed Res Int. 2015;2015:148651
43. Huang YH, Lin KH, Liao CH, Lai MW, Tseng YH, Yeh CT. Furin overexpression suppresses tumor growth and predicts a better postoperative disease-free survival in hepatocellular carcinoma. PLoS ONE. 2012;7:1–10.
44. Kosumi K, Hamada T, Zhang S, Liu L, da Silva A, Koh H, et al. Prognostic association of PTGS2 (COX-2) over-expression according to BRAF mutation status in colorectal cancer: results from two prospective cohorts and CALGB 89803 (Alliance) trial. Eur J Cancer. 2019;111:82–93.
45. Grabocka E, Bar-Sagi D. Mutant KRAS enhances tumor cell fitness by upregulating stress granules. Cell. 2016;167:1803–13.
46. Cordova ZM, Grönholm A, Kytölä V, Taverniti V, Hämäläinen S, Aittomäki S, et al. Myeloid cell expressed proprotein convertase FURIN attenuates inflammation. Oncotarget. 2016;7:54392–404.
47. Guo S, Liu M, Gonzalez-Perez RR. Role of Notch and its oncogenic signaling crosstalk in breast cancer. Biochim Biophys Acta —Rev Cancer. 2011;1815:197–213.
48. Batlle E, Massagué J. Transforming growth factor-β signaling in immunity and cancer. Immunity. 2019;50:924–40.
49. Chisanga D, Keerthikumar S, Pathan M, Ariyaratne D, Kalra H, Boukouris S, et al. Colorectal cancer atlas: an integrative resource for genomic and proteomic annotations from colorectal cancer cell lines and tissues. Nucleic Acids Res. 2016;44:D969–D974.
50. Louagie E, Taylor NA, Flamez D, Roebroek AJM, Bright NA, Meulemans S, et al. Role of furin in granular acidification in the endocrine pancreas: Identification of the V-ATPase subunit Ac45 as a candidate substrate. Proc Natl Acad Sci USA. 2008;105:12319–24.
51. Ramirez C, Hauser AD, Vucic EA, Bar-Sagi D. Plasma membrane V-ATPase controls oncogenic RAS-induced macropinocytosis. Nature. 2019;576:477–81.
52. Zhang Y, Zhou M, Wei H, Zhou H, He J, Lu Y, et al. Furin promotes epithelial-mesenchymal transition in pancreatic cancer cells via Hippo-YAP pathway. Int J Oncol. 2017;50:1352–62.
53. Couture F, Kwiatkowska A, Dory YL, Day R, Couture F, Kwiatkowska A, et al. Therapeutic uses of furin and its inhibitors: a patent review. Expert Opin Ther Pat. 2015;25:379–96.
54. Henrich S, Lindberg I, Bode W, Than ME. Proprotein convertase models based on the crystal structures of furin and kexin: Explanation of their specificity. J Mol Biol. 2005;345:211–27.
55. Susan-Resiga D, Essalmani R, Hamelin J, Asselin MC, Benjannet S, Chamberland A, et al. Furin is the major processing enzyme of the cardiac-specific growth factor bone morphogenetic protein 10. J Biol Chem. 2011;286:22785–94.
56. Ginefra P, Filippi BGH, Donovan P, Bessonnard S, Constam DB. Compartment-specific biosensors reveal a complementary subcellular distribution of bioactive furin and PC7. Cell Rep. 2018;22:2094–106.

UNCORRECTED PROOF

57. Hardes K, Becker GL, Lu Y, Dahms SO, Köhler S, Beyer W, et al. Novel furin inhibitors with potent anti-infectious activity. ChemMedChem. 2015;10:1218–31.
58. Löw K, Hardes K, Fedeli C, Seidah NG, Constam DB, Pasquato A et al. A novel cell-based sensor detecting the activity of individual basic proprotein convertases. FEBS J. 2019;1–24.
59. Dahms SO, Creemers JWM, Schaub Y, Bourenkov GP, Zögg T, Brandstetter H, et al. The structure of a furin-antibody complex explains non-competitive inhibition by steric exclusion of substrate conformers. Sci Rep. 2016;6:1–7.
60. Ghisoli M, Barve M, Mennel R, Lenarsky C, Horvath S, Wallraven G, et al. Three-year follow up of GMCSF/bi-shRNA(furin) DNA-transfected autologous tumor immunotherapy (Vigil) in metastatic advanced Ewing's Sarcoma. Mol Ther. 2016;24:1478–83.
61. Sarac MS, Cameron A, Lindberg I. The furin inhibitor hexa-D-arginine blocks the activation of Pseudomonas aeruginosa exotoxin a in vivo. Infect Immun. 2002;70:7136–9.
62. Blommaert E, Péanne R, Cherepanova NA, Rymen D, Staels F, Jaeken J, et al. Mutations in MAGT1 lead to a glycosylation disorder with a variable phenotype. Proc Natl Acad Sci. 2019;116:9865–70.
63. Ran FA, Hsu PD, Wright J, Agarwala V, Scott DA, Zhang F. Genome engineering using the CRISPR-Cas9 system. Nat Protoc. 2013;8:2281–308.
64. Tripathi S, Pohl MO, Zhou Y, Rodriguez-Frandsen A, Wang G, Stein DA, et al. Meta- and orthogonal integration of influenza 'OMICs' data defines a role for UBR4 in virus budding. Cell Host Microbe. 2015;18:723–35.
65. Jianjiong G, Bülent Arman A, Ugur D, Gideon D, Benjamin G, S Onur S, et al. Integrative analysis of complex cancer genomics and clinical profiles using the cBioPortal. Sci Signal. 2013;6:1–19.

UNCORRECTED PROOF

Journal : **41388**
Article : **1238**

SPRINGER NATURE

Author Query Form

Please ensure you fill out your response to the queries raised below and return this form along with your corrections

Dear Author

During the process of typesetting your article, the following queries have arisen. Please check your typeset proof carefully against the queries listed below and mark the necessary changes either directly on the proof/online grid or in the 'Author's response' area provided below

Queries	Details Required	Author's Response
AQ1	Please check your article carefully, coordinate with any co-authors and enter all final edits clearly in the eproof, remembering to save frequently. Once corrections are submitted, we cannot routinely make further changes to the article.	
AQ2	Note that the eproof should be amended in only one browser window at any one time; otherwise changes will be overwritten.	
AQ3	Author surnames have been highlighted. Please check these carefully and adjust if the first name or surname is marked up incorrectly. Note that changes here will affect indexing of your article in public repositories such as PubMed. Also, carefully check the spelling and numbering of all author names and affiliations, and the corresponding email address(es).	
AQ4	You cannot alter accepted Supplementary Information files except for critical changes to scientific content. If you do resupply any files, please also provide a brief (but complete) list of changes. If these are not considered scientific changes, any altered Supplementary files will not be used, only the originally accepted version will be published.	
AQ5	Please confirm that the edit to the sentence "Positive regulation of MAPK cascade..." preserves the originally intended meaning.	
AQ6	Please check the equation "[(D0 − DT=)/D0] × 100%" for clarity in the sentence "Cell migration towards the wound...".	
AQ7	Please provide volume number in reference 58.	

UNCORRECTED PROOF